

A Constraint Optimization Approach to Causal Discovery from Subsampled Time Series Data

Antti Hyttinen¹

HIIT, Department of Computer Science, University of Helsinki

Sergey Plis

Mind Research Network and University of New Mexico

Matti Järvisalo

HIIT, Department of Computer Science, University of Helsinki

Frederick Eberhardt

Humanities and Social Sciences, California Institute of Technology

David Danks

Department of Philosophy, Carnegie Mellon University

Abstract

We consider causal structure estimation from time series data in which measurements are obtained at a coarser timescale than the causal timescale of the underlying system. Previous work has shown that such subsampling can lead to significant errors in search for the system’s causal structure if not properly taken into account. In this paper, we first consider the search for system timescale causal structures that correspond to a given measurement timescale structure. We provide a constraint satisfaction procedure whose computational performance is several orders of magnitude better than previous approaches. We then consider finite-sample data as input, and propose the first constraint optimization approach for recovering system timescale causal structure. This algorithm optimally recovers from possible conflicts due to statistical errors. We then apply the method to real-world data, investigate the robustness and scalability of our method, consider further approaches to reduce underdetermination in the output, and perform an extensive comparison between different solvers on this inference problem. Overall, these advances build towards a full un-

Email addresses: antti.hyttinen@helsinki.fi (Antti Hyttinen), s.m.plis@gmail.com (Sergey Plis), matti.jarvisalo@helsinki.fi (Matti Järvisalo), fde@caltech.edu (Frederick Eberhardt), ddanks@cmu.edu (David Danks)

¹Corresponding author

derstanding of non-parametric estimation of system timescale causal structures from subsampled time series data.

Keywords: causality, causal discovery, graphical models, time series, constraint satisfaction, constraint optimization.

1. Introduction

Time-series data has long constituted the basis for causal modeling in many fields of science [12, 15, 22]. These data often provide very precise measurements at regular time points, but the underlying causal interactions that give rise to those measurements can occur at a much faster timescale than the measurement frequency. Time order information can simplify causal analysis since it can provide directionality, but time series data that undersamples the generating process can be misleading about the true causal connections [7, 19]. For example, Figure 1a shows the causal structure of a process unrolled over discrete time steps, and Figure 1c shows the corresponding structure of the same process, obtained by marginalizing every second time step. If we do not take into account the possibility of subsampling, then we might conclude that optimal control of V_2 requires interventions on both V_1 and V_3 , when the influence of V_3 on V_2 is, in fact, completely mediated by V_1 (and so intervening only on V_1 suffices).

Standard methods for estimating causal structure from time series either focus exclusively on estimating a transition model at the measurement timescale (e.g., Granger causality [12, 13]) or combine a model of measurement timescale transitions with so-called “instantaneous” or “contemporaneous” causal relations that aim to capture interactions that are faster than the measurement process (e.g., SVAR [22, 15, 18]), though only very specific types of interactions can be captured with these latter models. In contrast, we follow Plis et al. [30, 31] and Gong et al. [11], and explore the possibility of identifying (features of) the causal process at the true timescale from data that subsample this process.

In this paper, we provide an exact inference algorithm based on using a general-purpose Boolean constraint solver [4, 10], and demonstrate that it is orders of magnitudes faster than the current state-of-the-art method by Plis et al. [31]. At the same time, our approach is much simpler and, as we show, it allows inference in more general settings. We then develop the approach to integrate possibly conflicting constraints obtained from the data. In addition to an application of the method to the real-world data, we investigate the robustness and scalability of our method, consider further approaches to reduce underdetermination in the output and perform an extensive comparison between different solvers on this inference problem. Moreover, unlike the method by Gong et al. [11], our approach does not depend on a particular parameterization of the underlying model and scales to a more reasonable number of variables.

This article considerably extends a preliminary version presented at International Conference on Probabilistic Graphical Models 2016 (PGM 2016) [17].

40 Most noticeably, Sections 6–9 of this article provide entirely new contents, in-
 41 cluding a real-world case study (Section 6), an evaluation of the impact of the
 42 choice of constraint satisfaction and optimization solvers on the efficiency of the
 43 approach (Section 7), and a discussion on learning from mixed frequency data
 44 (Section 8). Furthermore, new simulations on accuracy and robustness (Section
 45 5, Figures 5-7) are now included.

46 2. Representation

47 We assume that the system of interest relates a set of variables $\mathbf{V}^t =$
 48 $\{V_1^t, \dots, V_n^t\}$ defined at discrete time points $t \in \mathbb{Z}$ with continuous ($\in \mathbb{R}^n$) or
 49 discrete ($\in \mathbb{Z}^n$) values [9]. We distinguish the representation of the true causal
 50 process at the *system timescale* from the time series data that are obtained at
 51 the *measurement timescale*. Following Plis et al. [31], we assume that the true
 52 between-variable causal interactions at the system timescale constitute a first-
 53 order Markov process; that is, that the independence $\mathbf{V}^t \perp\!\!\!\perp \mathbf{V}^{t-k} | \mathbf{V}^{t-1}$ holds
 54 for all $k > 1$. The parametric models for these causal structures are structural
 55 vector autoregressive (SVAR) processes or dynamic (discrete/continuous vari-
 56 able) Bayes nets. Since the system timescale can be arbitrarily fast (and causal
 57 influences take time), we assume that there is no “contemporaneous” causation
 58 of the form $V_i^t \rightarrow V_j^t$ [14]. We also assume that \mathbf{V}^{t-1} contains all common
 59 causes of variables in \mathbf{V}^t . These assumptions jointly express the widely used
 60 causal sufficiency assumption (see [35]) in the time series setting.

61 The system timescale causal structure can thus be represented by a causal
 62 graph G^1 (as in a dynamic Bayes net) with only $V_i^{t-1} \rightarrow V_j^t$ edges, where $i = j$
 63 is permitted (see Figure 1a for an example). Since the causal process is time-
 64 invariant, the edges repeat through t . In accordance with Plis et al. [31], for
 65 any G^1 we use a simpler, rolled graph representation, denoted by \mathcal{G}^1 , where
 66 $V_i \rightarrow V_j \in \mathcal{G}^1$ iff $V_i^{t-1} \rightarrow V_j^t \in G^1$. That is, the rolled graph represents time
 67 only implicitly in the edges, rather than through variable duplication. Figure 1b
 68 shows the rolled graph representation \mathcal{G}^1 of G^1 in Figure 1a.

69 Time series data are obtained from the above process at the *measurement*
 70 *timescale*, defined by some (possibly unknown) integral sampling rate u . The
 71 measured time series sample \mathbf{V}^t is at times $t, t - u, t - 2u, \dots$; we are interested
 72 in the case of $u > 1$, i.e., the case of subsampled data. A different route
 73 to subsampling would use continuous-time models as the underlying system
 74 timescale structure. However, some series (e.g., transactions such as salary
 75 payments) are inherently discrete-time processes [11], and many continuous-
 76 time systems can be approximated arbitrarily closely as discrete-time processes.
 77 Thus, we focus here on discrete-time causal structures as a justifiable, and yet
 78 simple, basis for our non-parametric inference procedure.

79 The structure of this subsampled time series can be obtained (leaving aside
 80 sampling variation) from G^1 by marginalizing the intermediate time steps. Fig-
 81 ure 1c shows the measurement timescale structure G^2 corresponding to sub-
 82 sampling rate $u = 2$ for the system timescale causal structure in Figure 1a.

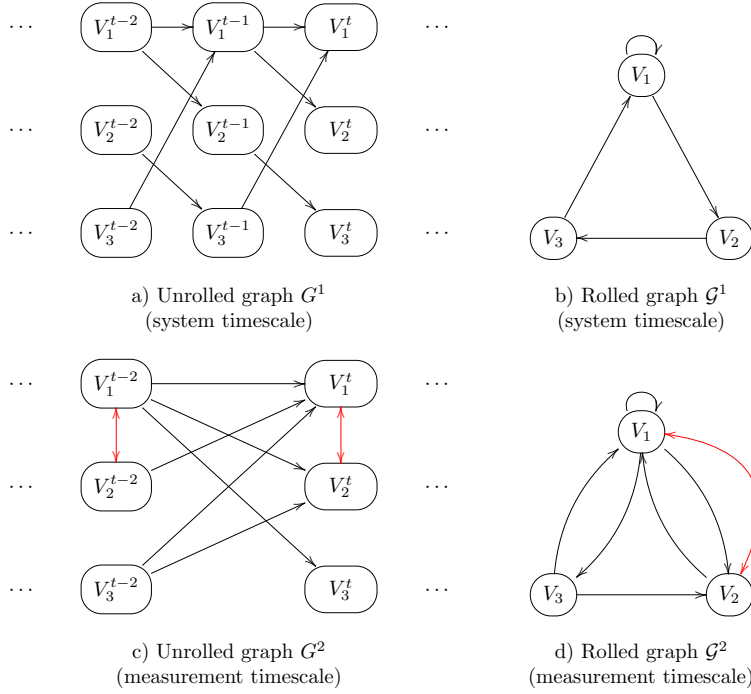


Figure 1: Example graphs with subsampling rate $u = 2$.

83 Each directed edge in G^2 corresponds to a directed path of length 2 in G^1 . For
 84 arbitrary u , the formal relationship between G^u and G^1 edges is

85
$$V_i^{t-u} \rightarrow V_j^t \in G^u \Leftrightarrow V_i^{t-u} \rightsquigarrow V_j^t \in G^1, \text{ where } \rightsquigarrow \text{ denotes a directed path.}^2$$

86 Subsampling a time series additionally induces “direct” dependencies be-
 87 tween variables in the same time step [37]. The bi-directed arrow $V_1^t \leftrightarrow V_2^t$ in
 88 Figure 1c is an example: V_1^{t-1} is an unobserved (in the data) common cause of
 89 V_1^t and V_2^t in G^1 (see Figure 1a). Formally, the system timescale structure G^1
 90 induces bi-directed edges in the measurement timescale G^u for $i \neq j$ as follows:

$$V_i^t \leftrightarrow V_j^t \in G^u \Leftrightarrow \exists (V_i^t \leftarrow V_c^{t-k} \rightsquigarrow V_j^t) \in G^1, k < u.$$

91 Just as \mathcal{G}^1 represents the rolled version of G^1 , \mathcal{G}^u represents the rolled version
 92 of G^u : $V_i \rightarrow V_j \in \mathcal{G}^u$ iff $V_i^{t-u} \rightarrow V_j^t \in G^u$ and $V_i \leftrightarrow V_j \in \mathcal{G}^u$ iff $V_i^t \leftrightarrow V_j^t \in G^u$.

93 The relationship between \mathcal{G}^1 and \mathcal{G}^u —that is, the impact of subsampling—

²We assume a type of faithfulness assumption (see [35]), such that influences along (multiple) paths between nodes do not exactly cancel in G^u .

94 can be concisely represented using only the rolled graphs:

$$V_i \rightarrow V_j \in \mathcal{G}^u \Leftrightarrow V_i \overset{u}{\rightsquigarrow} V_j \in \mathcal{G}^1 \quad (1)$$

$$V_i \leftrightarrow V_j \in \mathcal{G}^u \Leftrightarrow \exists (V_i \overset{<u}{\rightsquigarrow} V_c \overset{<u}{\rightsquigarrow} V_j) \in \mathcal{G}^1, i \neq j \quad (2)$$

95 where $\overset{u}{\rightsquigarrow}$ denotes a path of length u and $\overset{<u}{\rightsquigarrow}$ denotes a path shorter than u (of the
96 same length on each arm of a common cause). Using the rolled graph notation,
97 the logical encodings in Section 3 are considerably simpler.

98 Danks and Plis [6] demonstrated that, in the infinite sample limit, the causal
99 structure \mathcal{G}^1 at the system timescale is in general underdetermined, even when
100 the subsampling rate u is known and small. Consequently, even when ignor-
101 ing estimation errors, the most we can learn is an equivalence class of causal
102 structures at the system timescale. We define \mathcal{H} to be the estimated version of
103 \mathcal{G}^u , a graph over \mathbf{V} obtained or estimated at the measurement timescale (with
104 possibly unknown u). Due to underdetermination, multiple $\langle \mathcal{G}^1, u \rangle$ pairs can
105 imply \mathcal{H} , and so search is particularly challenging when u is unknown. At the
106 same time, if \mathcal{H} is estimated from data, it is possible, due to statistical errors,
107 that no \mathcal{G}^u has the same structure as \mathcal{H} . With these observations, we are ready
108 to define the computational problems focused on in this work.

109 **Task 1** *Given a measurement timescale structure \mathcal{H} (with possibly unknown*
110 *u), infer the (equivalence class of) causal structures \mathcal{G}^1 consistent with \mathcal{H} (i.e.*
111 *$\mathcal{G}^u = \mathcal{H}$ by Eqs. 1 and 2).*

112 We also consider the corresponding problem when the subsampled time series
113 is directly provided as input, rather than \mathcal{G}^u .

114 **Task 2** *Given a dataset of measurements of \mathbf{V} obtained at the measurement*
115 *timescale (with possibly unknown u), infer the (equivalence class of) causal*
116 *structures \mathcal{G}^1 (at the system timescale) that are (optimally) consistent with the*
117 *data.*

118 Section 3 provides a solution to Task 1, and Section 4 provides a solution to
119 Task 2. Later sections further consider generalizations of these two basic tasks.

120 3. Finding Consistent System Timescale Structures

121 We first focus on Task 1. We discuss the computational complexity of the
122 underlying decision problem, and present a practical Boolean constraint satis-
123 faction approach that empirically scales up to significantly larger graphs than
124 previous state-of-the-art algorithms.

125 3.1. On Computational Complexity

126 Consider the task of finding even a single \mathcal{G}^1 consistent with a given \mathcal{H} . A
127 variant of the associated decision problem is related to the NP-complete problem
128 of finding a matrix root.

129 **Theorem 1.** *Deciding whether there is a \mathcal{G}^1 that is consistent with the directed*
130 *edges of a given \mathcal{H} is NP-complete for any fixed $u \geq 2$.*

131 *Proof.* Membership in NP follows from a guess and check: guess a candidate
132 \mathcal{G}^1 , and deterministically check whether the length- u paths of \mathcal{G}^1 correspond to
133 the edges of \mathcal{H} [31]. For NP-hardness, for any fixed $u \geq 2$, there is a straight-
134 forward reduction from the NP-complete problem of determining whether a
135 Boolean B matrix³ has a u th root [21]: for a given $n \times n$ Boolean matrix B ,
136 interpret B as the directed edge relation of \mathcal{H} , i.e., \mathcal{H} has the edge (i, j) iff
137 $A^u(i, j) = 1$. It is then easy to see that there is a \mathcal{G}^1 that is consistent with the
138 obtained \mathcal{H} iff $B = A^u$ for some binary matrix A (i.e., a u th root of B). \square

139 If u is unknown, then membership in NP can be established in the same
140 way by guessing both a candidate \mathcal{G}^1 and a value for u . Theorem 1 ignores
141 the possible bi-directed edges in \mathcal{H} (whose presence/absence is also harder to
142 determine reliably from practical sample sizes; see Section 5). Knowledge of
143 the presences and absences of such edges in \mathcal{H} can restrict the set of candidate
144 \mathcal{G}^1 s. For example, in the special case where \mathcal{H} is known to not contain *any*
145 bi-directed edges, the possible \mathcal{G}^1 s have a fairly simple structure: in any \mathcal{G}^1
146 that is consistent with \mathcal{H} , every node has at most one successor.⁴ Whether this
147 knowledge can be used to prove a more fine-grained complexity result for special
148 cases is an open question.

149 3.2. A SAT-Based Approach

150 Recently, the first exact search algorithm for finding the \mathcal{G}^1 s that are consis-
151 tent with a given \mathcal{H} for a known u was presented by Plis et al. [31]; it represents
152 the current state-of-the-art. Their approach implements a specialized depth-
153 first search procedure for the problem, with domain-specific polynomial time
154 search-space pruning techniques. As an alternative, we present here a Boolean
155 satisfiability based approach. First, we represent the problem exactly using a
156 rule-based constraint satisfaction formalism. Then, for a given input \mathcal{H} , we
157 employ an off-the-shelf Boolean constraint satisfaction solver for finding a \mathcal{G}^1
158 that is guaranteed to be consistent with \mathcal{H} (if such \mathcal{G}^1 exists). Our approach is
159 not only simpler than the approach of Plis et al. [31], but as we will show, it
160 also significantly improves the current state-of-the-art in runtime efficiency and
161 scalability.

162 We present our approach using answer set programming (ASP) as the con-
163 straint satisfaction formalism⁵ [28, 33, 10]. It offers an expressive declarative
164 modeling language, in terms of first-order logical rules, for various types of NP-
165 hard search and optimization problems. To solve a problem via ASP, one first

³Multiplication of two values in $\{0, 1\}$ is defined as the logical-or, or equivalently, the maximum operator.

⁴To see this, assume X has two successors, Y and Z , s.t. $Y \neq Z$ in \mathcal{G}^1 . Then \mathcal{G}^u will contain a bi-directed edge $Y \leftrightarrow Z$ for all $u \geq 2$, which contradicts the assumption that \mathcal{H} has no bi-directed edges.

⁵Note the comparison to other solvers using the propositional SAT formalism in Section 7.

166 needs to develop an ASP program (in terms of ASP rules/constraints) that
 167 models the problem at hand; that is, the declarative rules implicitly represent
 168 the set of solutions to the problem in a precise fashion. Then one or multiple
 169 (optimal, in case of optimization problems) solutions to the original problem can
 170 be obtained by invoking an off-the-shelf ASP solver, such as the state-of-the-art
 171 **Clingo** system [10] used in this work. The search algorithms implemented in
 172 the **Clingo** system are extensions of state-of-the-art Boolean satisfiability and
 173 optimization techniques which can today outperform even specialized domain-
 174 specific algorithms, as we show here.

175 We proceed by describing a simple ASP encoding of the problem of finding
 176 a \mathcal{G}^1 that is consistent with a given \mathcal{H} . The input—the measurement timescale
 177 structure \mathcal{H} —is represented as follows. The input predicate `node/1` represents
 178 the nodes of \mathcal{H} (and all graphs), indexed by $1 \dots n$. The presence of a di-
 179 rected edge $X \rightarrow Y$ between nodes X and Y is represented using the predicate
 180 `edgeh/2` as `edgeh(X,Y)`. Similarly, the fact that an edge $X \rightarrow Y$ is not present
 181 is represented using the predicate `no_edgeh/2` as `no_edgeh(X,Y)`. The presence
 182 of a bidirected edge $X \leftrightarrow Y$ between nodes X and Y is represented using the
 183 predicate `confh/2` as `confh(X,Y)` ($X < Y$), and the fact that an edge $X \leftrightarrow Y$ is
 184 not present is represented using the predicate `no_confh/2` as `no_confh(X,Y)`.

185 If u is known, then it can be passed as input using `u(U)`; alternatively, it can
 186 be defined as a single value in a given range (here set to $1, \dots, 5$ as an example):

```
urange(1..5). % Define a range of u:s
1 { u(U): urange(U) } 1. % u(U) is true for only one U in the range
```

187 Solution \mathcal{G}^1 s are represented via the predicate `edge1/2`, where `edge1(X,Y)` is
 188 *true* iff \mathcal{G}^1 contains the edge $X \rightarrow Y$. In ASP, the set of candidate solutions (i.e.,
 189 the set of all directed graphs over n nodes) over which the search for solutions
 190 is performed, is declared via the so-called *choice construct* within the following
 191 rule, stating that candidate solutions may contain directed edges between any
 192 pair of nodes. If we have prior knowledge about edges that must (or must not)
 193 be present in \mathcal{G}^1 , then that content can straightforwardly be encoded here.

```
{ edge1(X,Y) } :- node(X), node(Y).
```

194 The implied measurement timescale structure \mathcal{G}^u for a candidate solution \mathcal{G}^1
 195 is represented using the predicates `edgeu(X,Y)` and `confu(X,Y)`, which are derived
 196 in the following way. First, we declare the mapping from a given \mathcal{G}^1 to the cor-
 197 responding \mathcal{G}^u by declaring the exact length- L paths in a non-deterministically
 198 chosen candidate solution \mathcal{G}^1 . For this, we declare rules that compute the length-
 199 L paths inductively for all $L \leq U$, using the predicate `path(X,Y,L)` to represent
 200 that there is a length- L path from X to Y .

```

% Derive all directed paths up to length U
path(X,Y,1) :- edge1(X,Y).
path(X,Y,L) :- path(X,Z,L-1), edge1(Z,Y), L <= U, u(U).

```

201 Second, to obtain \mathcal{G}^u , we encode Equations 1 and 2 with the following rules
202 that form predicates `edgeu/2` and `confu/2` describing the edges \mathcal{G}^1 induces on
203 the measurement timescale structure.

```

% Paths of length U, correspond to measurement timescale edges
edgeu(X,Y) :- path(X,Y,L), u(L).

% Paths of equal length (<U) from a single node result in bi-directed edges
confu(X,Y) :- path(Z,X,L), path(Z,Y,L), node(X;Y;Z), X < Y, L < U, u(U).

```

204 Finally, we declare constraints that require that the \mathcal{G}^u represented by the
205 `edgeu/2` and `confu/2` predicates is consistent with the input \mathcal{H} . This is achieved
206 with the following rules, which enforce that the edge relations of \mathcal{G}^u and \mathcal{H} are
207 exactly the same for any solution \mathcal{G}^1 .

```

:- edgeh(X,Y), not edgeu(X,Y).
:- no_edgeh(X,Y), edgeu(X,Y).
:- confh(X,Y), not confu(X,Y).
:- no_confh(X,Y), confu(X,Y).

```

208 Our ASP encoding of Task 1 consists of the rules just described. The set of
209 solutions of the encoding correspond exactly to the \mathcal{G}^1 s consistent with the
210 input \mathcal{H} .

211 3.3. Runtime Comparison

212 Both our proposed SAT-based approach and the recent specialized search
213 algorithm MSL of Plis et al. [31] are correct and complete, so we focus on dif-
214 ferences in efficiency, using the implementation of MSL by the original authors.
215 Our approach allows for searching simultaneously over a range of values of u ,
216 but Plis et al. [31] focused on the case $u = 2$; hence, we restrict the comparison
217 to $u = 2$.

218 We simulated system timescale graphs with varying density and number of
219 nodes (see Section 5 for exact details), and then computed the implied mea-
220 surement timescale structures for subsampling rate $u = 2$. This structure was
221 given as input to the inference procedures. Note that the input consisted here
222 of graphs for which there always is a \mathcal{G}^1 , so all instances were satisfiable. The
223 task of the algorithms was to output up to 1000 (system timescale) graphs in
224 the equivalence class. The ASP encoding was solved by `Clingo` using the flag
225 `-n 1000` for the solver to enumerate 1000 solution graphs (or all, in cases where
226 there were fewer than 1000 solutions).

227 The running times of the MSL algorithm and our approach (SAT) on 10-
228 node input graphs with different edge densities are shown in Figure 2 (left).

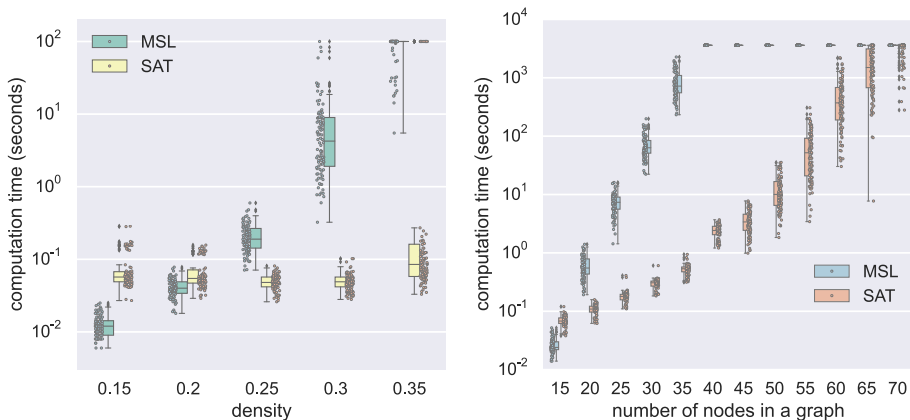


Figure 2: Running times. Left: for 10-node graphs as a function of graph density (100 graphs per density and a timeout of 100 seconds); Right: for 10%-dense graphs as a function of graph size (100 graphs per density and a timeout of 1 hour).

229 Figure 2 (right) shows the scalability of the two approaches in terms of increasing
 230 number of nodes in the input graphs and fixed 10% edge density. Our declarative
 231 approach clearly outperforms MSL. 10-node input graphs, regardless of edge
 232 density, are essentially trivial for our approach, while the performance of MSL
 233 deteriorates noticeably as the density increases. For varying numbers of nodes
 234 in 10% density input graphs, our approach scales up to 65 nodes with a one hour
 235 time limit; even for 70 nodes, 25 graphs finished in one hour. In contrast, MSL
 236 reaches only 35 nodes; our approach uses only a few seconds for those graphs.
 237 The scalability of our algorithm allows for investigating the influence of edge
 238 density for larger graphs. Figure 3 (left) plots the running times of our approach
 239 (when enumerating *all* solutions) for $u = 2$ on 20-node input graphs of varying
 240 densities. Note that here the instances are sorted by the running time for each
 241 individual density (curve). With a time limit of 1000 seconds we can solve 80%
 242 of the instances with 26% density, almost all of the instances with 25% density
 243 and all of the instances with 24% density. Thus, the running time is increased
 244 for denser graphs: in addition to more constraints, there are also more members
 245 in the equivalence classes. Finally, Figure 3 (right) shows the scalability of our
 246 approach in the more challenging task of enumerating *all* solutions over the
 247 range $u = 1, \dots, 5$ simultaneously. This also demonstrates the generality of our
 248 approach: it is not restricted to solving for individual values of u separately.

249 4. Learning System Timescale Structures from Data

250 Due to statistical errors in estimating \mathcal{H} and the sparse distribution of im-
 251 plied \mathcal{G}^u in the space of possible undersampled graphs, the estimated \mathcal{H} will
 252 often have *no* \mathcal{G}^1 s with $\mathcal{G}^u = \mathcal{H}$. Given such an \mathcal{H} , neither the MSL algorithm
 253 nor our approach in the previous section can output a solution, and they simply

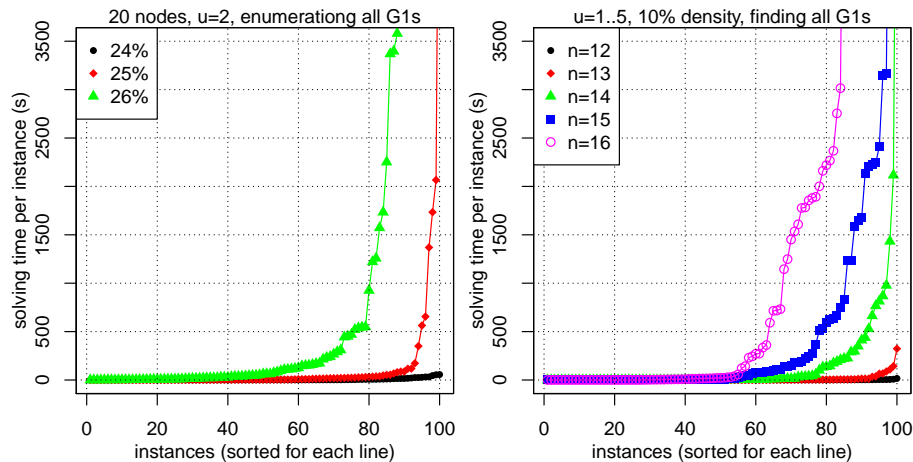


Figure 3: Top: Influence of input graph density on running times of our approach. Bottom: Scalability of our approach when enumerating all solutions over $u = 1, \dots, 5$.

254 conclude that no solution \mathcal{G}^1 exists for the input \mathcal{H} . In terms of our constraint
 255 declarations, this is witnessed by conflicts among the constraints and the under-
 256 lying model space for any possible solution candidate. Given the inevitability
 257 of statistical errors, we should not simply conclude that no consistent \mathcal{G}^1 exists
 258 for such an \mathcal{H} . Rather, we should aim to learn \mathcal{G}^1 s that, in light of the under-
 259 lying conflicts, are “optimally close” (in some well-defined sense of “optimal”)
 260 to being consistent with \mathcal{H} . We now turn to this more general problem set-
 261 ting, and propose what (to the best of our knowledge) is the first approach to
 262 learning, by employing constraint optimization, from undersampled data under
 263 conflicts.⁶ In fact, we can use the ASP formulation already discussed—with
 264 minor modifications—to address this problem.

265 In this more general setting, the input consists of both the estimated graph
 266 \mathcal{H} , and also (i) weights $w(e \in \mathcal{H})$ indicating the reliability of edges present in \mathcal{H} ;
 267 and (ii) weights $w(e \notin \mathcal{H})$ indicating the reliability of edges absent in \mathcal{H} . Since
 268 \mathcal{G}^u is \mathcal{G}^1 subsampled by u , the task is to find a \mathcal{G}^1 that minimizes the objective
 269 function:

$$f(\mathcal{G}^1, u) = \sum_{e \in \mathcal{H}} I[e \notin \mathcal{G}^u] \cdot w(e \in \mathcal{H}) + \sum_{e \notin \mathcal{H}} I[e \in \mathcal{G}^u] \cdot w(e \notin \mathcal{H}),$$

270 where the indicator function $I(c) = 1$ if the condition c holds, and $I(c) = 0$
 271 otherwise. Thus, edges that differ between the estimated input \mathcal{H} and the
 272 \mathcal{G}^u corresponding to the solution \mathcal{G}^1 are penalized by the weights representing
 273 the reliability of the measurement timescale estimates. In the following, we first

⁶Given conflicts, Plis et al. [31] simply ran the MSL algorithm on graphs close to \mathcal{H} , which is not guaranteed to find an optimal solution, nor does it scale computationally.

274 outline how to generalize the ASP encoding from the preceding section to enable
 275 search for optimal \mathcal{G}^1 with respect to this objective function. We then describe
 276 two alternatives for determining the weights w . In the following section, we
 277 present simulation results on the relative performance of the different weighting
 278 schemes.

279 4.1. Learning by Constraint Optimization

280 To model the objective function for handling conflicts, only simple modifi-
 281 cations are needed to our ASP encoding: instead of declaring *hard* constraints
 282 that require that the paths induced by \mathcal{G}^1 *exactly* correspond to the edges in
 283 \mathcal{H} , we *soften* these constraints by declaring that the violation of each individual
 284 constraint incurs the associated weight as penalty. In the ASP language, this
 285 can be expressed by augmenting the input predicates `edgeh(X,Y)` with weights:
 286 `edgeh(X,Y,W)` (and similarly for `no_edgeh`, `confh` and `no_confh`). Here the addi-
 287 tional argument W represents the weight $w((x \rightarrow y) \in \mathcal{H})$ given as input. The
 288 following expresses that each conflicting presence of an edge in \mathcal{H} and \mathcal{G}^u is
 289 penalized with the associated weight W .

```

:~ edgeh(X,Y,W), not edgeu(X,Y). [W,X,Y,1]
:~ no_edgeh(X,Y,W), edgeu(X,Y). [W,X,Y,1]
:~ confh(X,Y,W), not confu(X,Y). [W,X,Y,2]
:~ no_confh(X,Y,W), confu(X,Y). [W,X,Y,2]

```

290 This modification provides an ASP encoding for Task 2; that is, the optimal
 291 solutions to this ASP encoding correspond exactly to the \mathcal{G}^1 s that minimize the
 292 objective function $f(\mathcal{G}^1, u)$ for given u and input \mathcal{H} with weighted edges.

293 4.2. Weighting Schemes

294 We use two different schemes for weighting the presences and absences of
 295 edges in \mathcal{H} according to their reliability. To determine the presence/absence of
 296 an edge $X \rightarrow Y$ in \mathcal{H} , we simply test the corresponding independence $X^{t-1} \perp\!\!\!\perp$
 297 $Y^t \mid \mathbf{V}^{t-1} \setminus X^{t-1}$. To determine the presence/absence of an edge $X \leftrightarrow Y$ in \mathcal{H} ,
 298 we run the independence test: $X^t \perp\!\!\!\perp Y^t \mid \mathbf{V}^{t-1}$.

299 The simplest approach is to use uniform weights for the estimated \mathcal{H} :

$$\begin{aligned}
 w(e \in \mathcal{H}) &= 1 \quad \forall e \in \mathcal{H}, \\
 w(e \notin \mathcal{H}) &= 1 \quad \forall e \notin \mathcal{H}.
 \end{aligned}$$

300 Uniform edge weights resemble the search on the Hamming cube of \mathcal{H} that Plis
 301 et al. [31] used to address the problem of finding \mathcal{G}^1 s when \mathcal{H} did not correspond
 302 to any \mathcal{G}^u , though our approach is much superior computationally.

303 A more intricate approach is to use pseudo-Bayesian weights following [16,
 304 34, 24]. They used Bayesian model selection to obtain reliability weights for
 305 independence tests. Instead of a p -value and a binary decision, these types of
 306 tests give a measurement of reliability for an independence/dependence state-
 307 ment as a Bayesian probability. We can directly incorporate their approach of

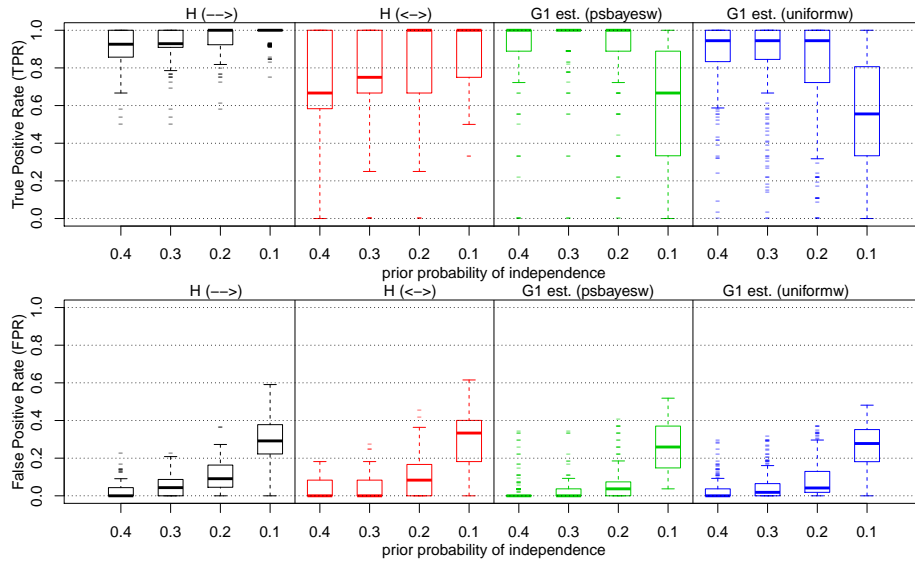


Figure 4: Accuracy of the optimal solutions when $u = 2$ with different weighting schemes and parameters (on x-axis). See text for further details.

308 using log-probabilities as the reliability weights for the edges. For details, see
 309 Section 4.3 of Hyttinen et al. [16]. Again, we only compute weights for the
 310 independence tests mentioned above in the estimation of \mathcal{H} .

311 5. Simulations

312 We use simulations to explore the accuracy and runtime efficiency of our
 313 approach in various different settings. For the simulations, system timescale
 314 structures \mathcal{G}^1 and the associated data generating models were constructed in
 315 the following way. To guarantee connectedness of the graphs, we first formed
 316 a cycle of all nodes in a random order (following Plis et al. [31]). We then
 317 randomly sampled additional directed edges until the required density was obtained.
 318 Recall that there are no bidirected edges in \mathcal{G}^1 . We used Equations 1
 319 and 2 to generate the measurement timescale structure \mathcal{G}^u for a given u . When
 320 sample data were required, we used linear Gaussian structural autoregressive
 321 processes (order 1) with structure \mathcal{G}^1 to generate data at the system timescale,
 322 where coefficients were sampled from the two intervals $\pm[0.2, 0.8]$. We then
 323 discarded intermediate samples⁷ to get the particular subsampling rate.⁸

⁷All sample counts refer to the number of samples after subsampling.

⁸Clingo only accepts integer weights; we multiplied weights by 1000 and rounded to the nearest integer.

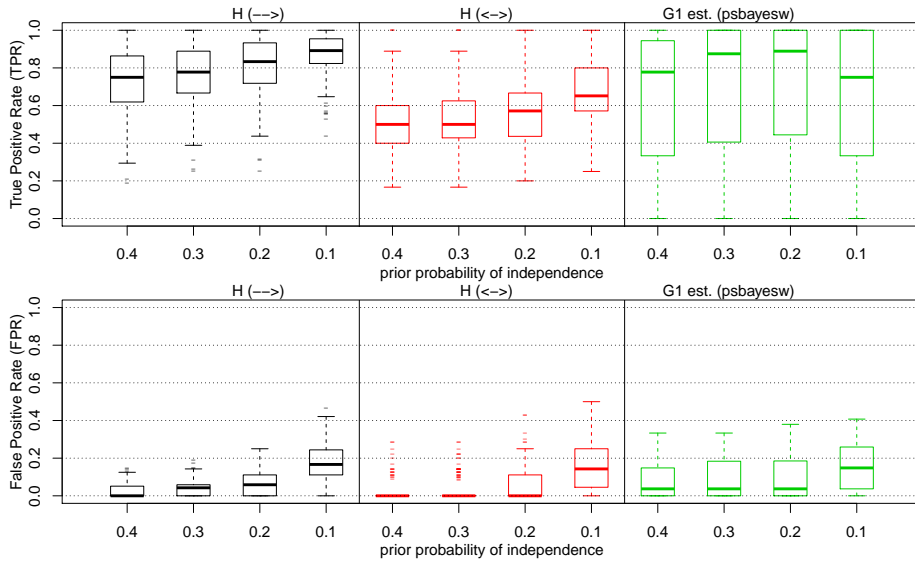


Figure 5: Accuracy of the optimal solutions when $u = 3$. See text for further details.

324 *5.1. Accuracy*

325 Figure 4 shows the accuracy of the different methods in one setting: subsam-
 326 pling rate $u = 2$, network size $n = 6$, average degree 3 (density 25%), sample
 327 size $N = 250$, and 200 datasets in total. The positive predictions correspond
 328 to presences of edges; when the method returned several solutions with equal
 329 cost, we used the mean solution accuracy to measure the output accuracy. The
 330 x-axis numbers correspond to the adjustment parameter for the statistical inde-
 331 pendence tests (prior probability of independence). The two left columns
 332 (black and red) show the true positive rate and false positive rate of the \mathcal{H}
 333 estimation (compared to the true \mathcal{G}^2), for the different types of edges, using dif-
 334 ferent statistical tests. Given 250 samples, we see that the structure of \mathcal{G}^2 can
 335 be estimated with a good tradeoff of TPR and FPR with the middle parameter
 336 values, but not perfectly. The presence of directed edges can be estimated more
 337 accurately. More importantly, the two rightmost columns in Figure 4 (green
 338 and blue) show the accuracy of the \mathcal{G}^1 estimation. Both weighting schemes pro-
 339 duce good accuracy for the middle parameter values, although there are some
 340 outliers. The pseudo-Bayesian weighting scheme still outperforms the uniform
 341 weighting scheme, as it produces high TPR with low FPR for a range of thresh-
 342 old parameter values (especially for 0.3).

343 Figure 5 shows the accuracy when $u = 3$, $n = 6$, average degree 3 (den-
 344 sity 25%), $N = 500$, and 200 datasets. The accuracy for edge presences in the
 345 measurement timescale graph \mathcal{H} is lower than for $u = 2$, even though we have
 346 twice the number of samples (Figure 5, black, red). The problem is that mea-
 347 surement timescale edges here correspond to 3-edge paths, whose causal effects

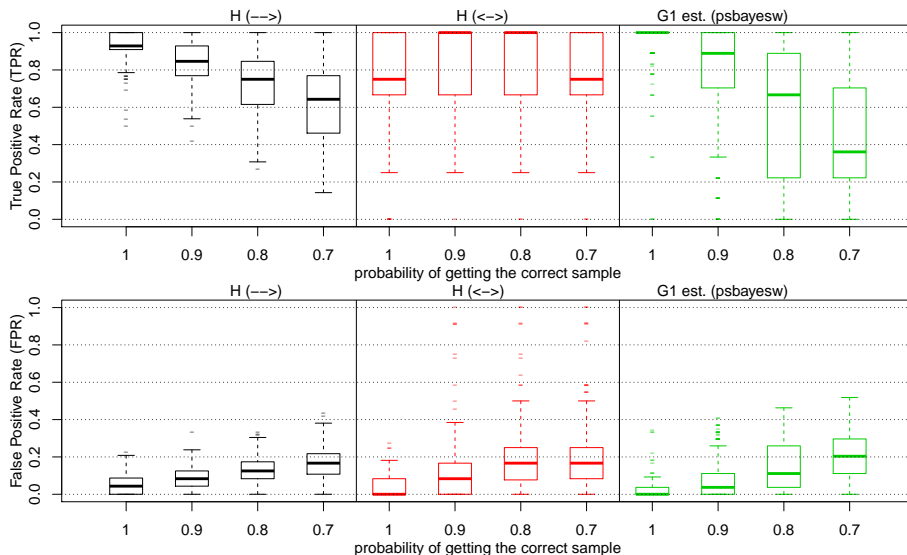


Figure 6: Accuracy of the optimal solutions when $u = 2$ and some samples are obtained at the adjacent timepoints.

348 will be smaller (on average) than 2-edge paths for a fixed interval of system
 349 timescale edge coefficients ($\pm[0.2, 0.8]$), and so are harder to detect. Neverthe-
 350 less, the constraint optimization procedure achieves a good tradeoff between
 351 TPR and FPR for system timescale edges (Figure 5, green). Larger subsam-
 352 pling rates (u) require more samples for accurate \mathcal{G}^1 structure discovery, but
 353 not several orders of magnitude more data.

354 5.2. Robustness of the subsampling rate

355 Figure 6 shows the accuracy of this method when some of the samples are not
 356 obtained at the exact time assumed by the measurement timescale. Specifically,
 357 the x-axis specifies the probability with which we obtain the correct sample (for
 358 the given $u = 2$); otherwise, we take either the sample before or the sample
 359 after (synchronously for all variables), splitting the remaining probability. The
 360 results with probability 1 equal the result in Figure 4 with prior probability
 361 of independence 0.3 and a sample size of $N = 250$. These values were used
 362 in all runs in this plot. Unsurprisingly, as the “jitter” in the sampling process
 363 increases, the results deteriorate in terms of TPR and FPR. However, at least
 364 for the models and subsampling rate of $u = 2$ tested here, the inference is not
 365 overly sensitive. When the probability of a correct sample is 0.9, the results
 366 are still quite good, alleviating somewhat the dependence on the assumption
 367 of an exact subsampling rate. Naturally, there are many further permutations
 368 one could explore: jitter could affect variables independently of one another,
 369 jitter could be represented by a more complex distribution, we could explore
 370 the effect of jitter for different subsampling rates or when the subsampling rate

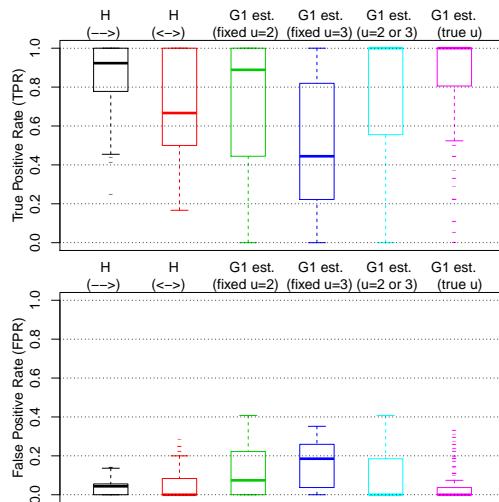


Figure 7: Accuracy when the true u is unknown. Two left boxplots show accuracy of the H estimate as before. The next three boxplots show the accuracy of our approach when, regardless of the true u , u is fixed to 2, or to 3, or left for the procedure decision, respectively. In the rightmost boxplot the true u was given as input.

371 is unknown. Moreover, jitter could have a persistent, rather than a local effect,
 372 in shifting subsequent measures as well. We have here only explored the very
 373 simple case mimicking the situation where the measurement device as a whole
 374 (i.e. simultaneously for all variables) comes out of synch with the system at
 375 random points without consequences for subsequent samples.

376 Figure 7 further examines the possibility to distinguish between different
 377 subsampling rates. We generated 500 samples of data from 200 models (average
 378 degree 3) with equal numbers of cases with $u = 2$ or $u = 3$. The two leftmost
 379 boxplots show the accuracy of the estimated H , which, given the mixture of $u =$
 380 2 and $u = 3$, is between the accuracy of H obtained in previous simulations. The
 381 next two boxplots show the accuracy of the G_1 estimate, when the subsampling
 382 rate u for the search procedure is fixed to 2 or 3, respectively, regardless of the
 383 true u . As expected, the accuracy is mediocre in this case, since the method
 384 assumes the incorrect subsampling rate u in half of the runs. But when the
 385 method is left to determine the correct u itself, the accuracy improves again,
 386 as shown in the boxplots second from the right (the method was run with
 387 $u = 2..3$). In fact, the accuracy comes close to that of the rightmost boxplots,
 388 where the correct u was given as input to the procedure. Thus the procedure
 389 is often able to recognize the correct u . The longer tails indicate that at times
 390 the determination of u is not perfect.

391 5.3. Scalability

392 Finally, the running times of our approach are shown in Figure 8 with differ-
 393 ent weighting schemes, network sizes (n), and sample sizes (N). The subsam-

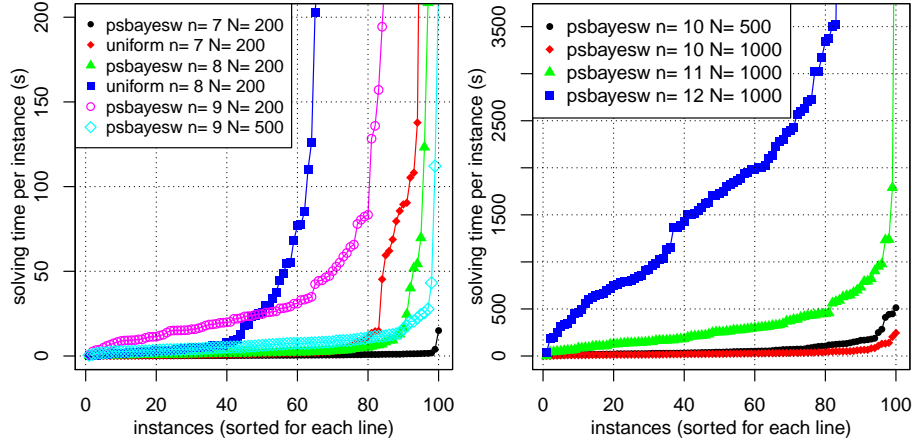


Figure 8: Scalability of our approach under different settings.

394 pling rate was again fixed to $u = 2$, and average node degree was 3. Figure 8
 395 (left) shows that the pseudo-Bayesian weighting scheme allows for much faster
 396 solving: for $n = 7$, it finishes all runs in a few seconds (black line), while the
 397 uniform weighting scheme (red line) takes several minutes in the longest runs.
 398 Thus, the pseudo-Bayesian weighting scheme provides the best performance in
 399 terms of both computational efficiency and accuracy. The sample size has a
 400 significant effect on the running times: larger sample sizes take *less* time. Runs
 401 for $n = 9, N = 200$ (blue line) take longer than for $n = 9, N = 500$ (Figure 8
 402 left, magenta vs. cyan lines). Intuitively, statistical tests should be more ac-
 403 curate with larger sample sizes, resulting in fewer conflicting constraints. For
 404 $N = 1000$, the global optimum is found here for up to 12-node graphs (Figure 8
 405 right), though in a considerable amount of time.

406 6. Case Study: House data of Peters et al. [29]

407 In order to demonstrate the applicability to real-world data, we analyzed
 408 the house temperature and humidity data of Peters et al. [29]. The data in-
 409 cludes 7265 samples of hourly temperature and humidity measurements of six
 410 sensors placed in a house (SHED=in the shed, OUT=outside, KIT=kitchen
 411 boiler, LIV=living room, WC=wc, BATH=bathroom) in the Black Forest. The
 412 house has heating, but the house is not in use for most of the year. This data
 413 was also partly analyzed by Gong et al. [11]. The measurements of this system
 414 were obtained at coarser intervals than the process of temperature and humidity
 415 changes are thought to take place. Since the data includes outside temperature
 416 and humidity measurements, the assumption of causal sufficiency at the system
 417 timescale seems a good approximation.

418 We analyzed the temperature and humidity components separately, and ex-

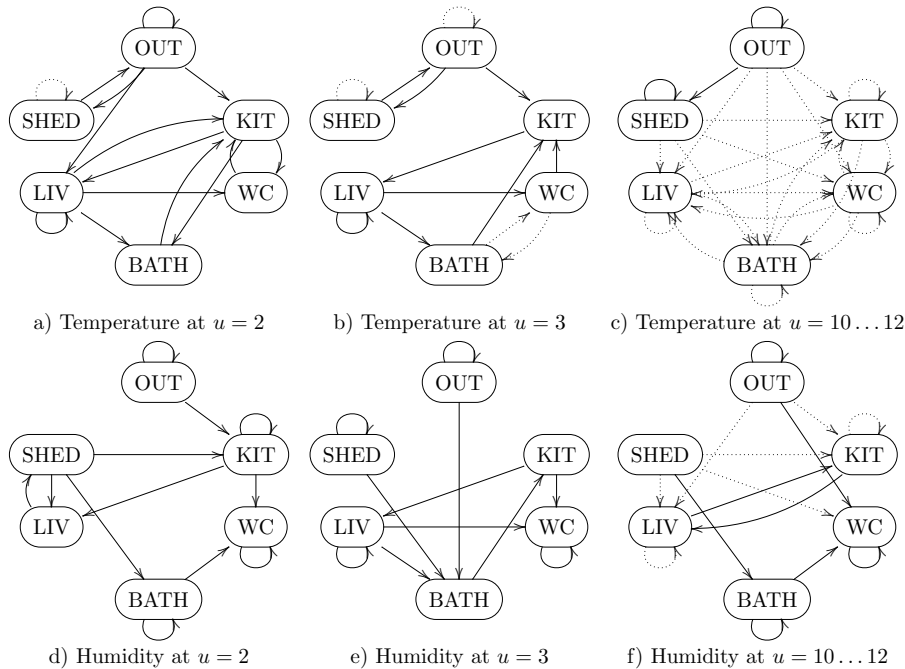


Figure 9: Results of the House data analysis. Edges with full lines are found to be present, absent edges are found to be absent, edges with dotted lines may be present or absent.

419 amined the differences of sequential measurements,⁹ as this removed trends from
 420 each univariate time series. The temperature measurement timescale graph (ob-
 421 tained at 0.9 prior probability of independence) includes a total of 20 (out of
 422 36) directed edges, and 8 (out of 15) bidirected edges, with varying pseudo-
 423 Bayesian weights. The humidity measurement timescale graph had the same
 424 total numbers of edges, although not the exact same edges.

425 As explained earlier, subsampling introduces underdetermination of the sys-
 426 tem timescale graph. Thus, we determined the presence of individual system
 427 timescale edges in the following way [23]. For each edge in \mathcal{G}^1 , we ran the in-
 428 ference procedure first enforcing its presence and then enforcing its absence.¹⁰
 429 The difference in objective function values for the two outputs—the optimal \mathcal{G}^1 s
 430 that do or do not contain the edge, respectively—indicates the support for the
 431 presence (absence) of the edge.

432 For the estimated \mathcal{H} , we computed \mathcal{G}^1 s edgewise for subsampling rates of
 433 $u = 2, 3$. (Since the measurements were hourly, these correspond to time steps
 434 of 30 and 20 minutes, respectively.) The two temperature graphs for $u = 2$
 435 and $u = 3$ (Figure 9a,b) differ substantially from one another, as do the two

⁹This may take out some of the influences selfloops would induce.

¹⁰This can be done by adding a simple clause to the input code “`edge(X,Y).`” to force the presence and “`:-edge1(X,Y).`” to enforce the absence of $X \rightarrow Y$.

436 humidity graphs (Figure 9d,e). These results provide empirical demonstrations
437 of the impact of subsampling, as different choices of u imply different structures.
438 At the same time, timesteps of 20 and 30 minutes arguably do not correspond
439 to realistic time steps for the temperature and humidity changes measured by
440 these data.

441 We thus considered larger subsampling rates $u = 10 \dots 12$, which correspond
442 to more realistic time steps of 5-6 minutes. As expected, there is more under-
443 determination for these u , but the results are also more plausible. Figure 9c
444 suggests that the temperature outside is not directly influenced by the temper-
445 ature in any of the rooms, but it directly influences the temperature in the shed.
446 The data do not, however, uniquely determine how the outside temperature di-
447 rectly affects the temperatures in the rooms inside the house, nor the system
448 timescale causal dependencies between temperatures in the rooms.

449 Similarly, the humidity structures for larger u are more plausible. Figure 9f
450 suggests that the humidity level in the WC is driven by both bathroom and
451 outside humidity, which is sensible since the WC is located next to the bathroom
452 and has a window, according to Peters et al. [29]. In contrast, it seems unrealistic
453 that the shed humidity would affect bathroom humidity as suggested by the
454 graph. It is possible that the humidity in the shed provides information on the
455 outside humidity, and so is mistaken for it. (We note that outside and shed
456 measurements are also mixed in some results of Peters et al. [29].) The living
457 room and kitchen boiler humidities seem to depend on each other directly, so
458 the data suggest that the rooms may be adjacent, though that information was
459 not provided by Peters et al. [29].

460 Overall, the processes controlling the temperature and humidity have dif-
461 ferences and similarities. Determining the placement of sensors thus seems to
462 require data from both measurements types.

463 7. Solver Performance Comparison

464 Thus far in this article we have considered `Clingo` as the only solver to
465 find solutions to a declarative constraint encoding of the computational prob-
466 lems considered here. This raises the question to what extent the choice of
467 the constraint solver affects the runtime performance of our approach. While
468 the high-level ASP syntax is relatively easy to understand and modify, our ap-
469 proach can also be represented via propositional logic. The benefit of using
470 propositional logic is that various SAT solvers, as well as MaxSAT solvers (as
471 the Boolean optimization generalization of SAT), can be applied directly. In
472 this section we evaluate the impact of the choice of SAT and MaxSAT solvers
473 on the runtime efficiency of our approach.

474 7.1. Direct Propositional SAT Encoding

475 A direct propositional SAT encoding for finding a system timescale causal
476 structure \mathcal{G}^1 consistent with a measurement timescale graph \mathcal{H} for a known u
477 is presented in Eqs. 3–10.

$$\vec{h}_{X,Y} \quad \forall X, Y \in \mathbf{V} : X \rightarrow Y \in \mathcal{H} \quad (3)$$

$$\neg \vec{h}_{X,Y} \quad \forall X, Y \in \mathbf{V} : X \rightarrow Y \notin \mathcal{H} \quad (4)$$

$$\leftrightarrow h_{X,Y} \quad \forall X, Y \in \mathbf{V} : X < Y, X \leftrightarrow Y \in \mathcal{H} \quad (5)$$

$$\neg \leftrightarrow h_{X,Y} \quad \forall X, Y \in \mathbf{V} : X < Y, X \leftrightarrow Y \notin \mathcal{H} \quad (6)$$

$$\vec{h}_{X,Y} \Leftrightarrow \bigvee_{Z \in \mathbf{V}} (p_{X,Z}^{u-1} \wedge p_{Z,Y}^1) \quad \forall X, Y \in \mathbf{V} \quad (7)$$

$$p_{X,Y}^{l+1} \Leftrightarrow \bigvee_{Z \in \mathbf{V}} (p_{X,Z}^l \wedge p_{Z,Y}^1) \quad \forall X, Y \in \mathbf{V}, l \in \{1..u-2\} \quad (8)$$

$$\leftrightarrow h_{X,Y} \Leftrightarrow \bigvee_{l=1}^{u-1} \leftrightarrow h_{X,Y}^l \quad \forall X, Y \in \mathbf{V} : X < Y \quad (9)$$

$$\leftrightarrow h_{X,Y}^l \Leftrightarrow \bigvee_{Z \in \mathbf{V}} (p_{Z,X}^l \wedge p_{Z,Y}^1) \quad \forall X, Y \in \mathbf{V} : X < Y, l \in \{1..u-1\} \quad (10)$$

478 Essentially, Eqs. 3–6 enforce the input constraints imposed by \mathcal{H} . Following the
 479 ASP encoding presented earlier, Eqs. 7–10 encode the mapping from the \mathcal{G}^1 's—
 480 the edge relation of which is encoded as the length-1-path variables $p_{X,Y}^1$ —that
 481 are consistent with \mathcal{H} .

482 7.2. Solver Comparison: Finding Consistent System Timescale Structures

483 The results of a runtime performance comparison between Clingo and two
 484 state-of-the-art SAT solvers, Glucose [2] and Lingeling [3], is presented in Fig-
 485 ure 10 for $u = 3$, edge density of 10% and the numbers of nodes ranging from
 486 27 (on left) to 30 (on right). Note that the plots give the running times of
 487 each of the three solvers sorted individually for each solver. In terms of runtime
 488 performance, the SAT solvers Glucose and Lingeling, both working directly on
 489 the propositional SAT encoding, exhibit noticeably improved performance over
 490 Clingo as the number of nodes is increased (right plot). Thus, in terms of run-
 491 time efficiency of our approach, it can be beneficial to apply current and future
 492 advances in state-of-the-art SAT solvers directly on the propositional level for
 493 improved performance. In these simulations the ASP paradigm does not show
 494 any particular computational advantage.

495 7.3. Solver Comparison: Learning System Timescale Structures from Data

496 As with the ASP encoding given earlier, the SAT encoding given as Eqs. 3–
 497 10 is easily extended to solve the optimization problem underlying the task of
 498 learning system timescale structure from undersampled data. In the language of
 499 MaxSAT, the only change required is to make the constraints in Eqs. 3–6 soft,
 500 and to declare that the cost incurred from not satisfying these individual con-
 501 straints equals that of $w(e \in \mathcal{H})$ (for Eqs. 3,5) or $w(e \notin \mathcal{H})$ (for Eqs. 4,6) for the

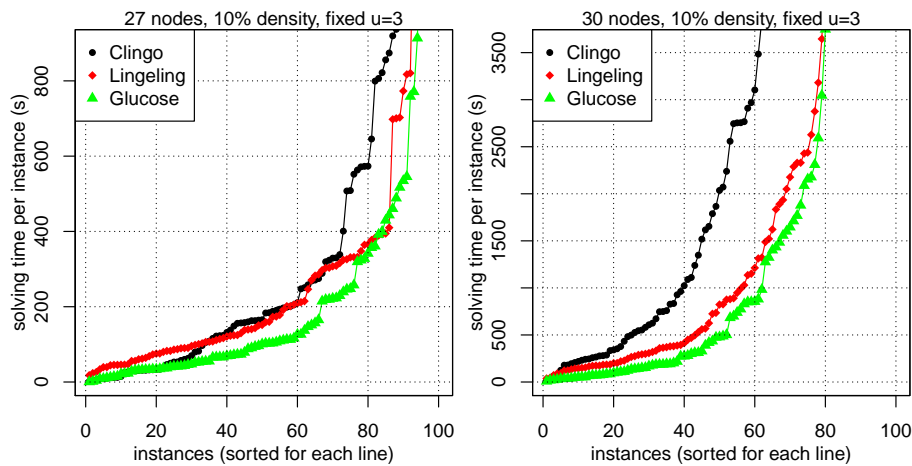


Figure 10: Comparison of running times for different solvers finding a single graph in the equivalence class.

502 corresponding edge e . This enables a comparison of the runtime performance of
 503 Clingo’s default branch-and-bound based search for an optimal solution to those
 504 of other MaxSAT solvers implementing alternative algorithmic approaches on
 505 the direct propositional MaxSAT encoding. Results comparing the performance
 506 of Clingo to that of the modern MaxSAT solvers Eva500a [27], LMHS [32],
 507 MSCG [26], Open-WBO [25], PrimalDual [5], and QMaxSAT [20], as well as
 508 the commercial integer programming (IP) solver CPLEX run on a standard
 509 IP translation of MaxSAT [8, 1], are shown in Figure 11. Here we observe
 510 that Clingo’s branch-and-bound approach is among the best performing solvers
 511 (with the considered problem parameters). However, the results also suggest
 512 that QMaxSAT, and so-called model-based approaches using a SAT solver to
 513 search for an optimal solution over the objective function range with a top-down
 514 strategy, can improve on the runtime efficiency of our approach. These results
 515 clearly show that the choice of the underlying Boolean optimization solver can
 516 indeed have a noticeable influence on the practical efficiency of the approach.
 517 There is at least some potential for further improving the runtime performance
 518 of our approach by making use of advances in MaxSAT solver technology.

519 8. Learning from Mixed Frequency Data

520 In some contexts we may have obtained data from the same system at dif-
 521 ferent subsampling frequencies. Two cases can be distinguished here: First, the
 522 subsampled time series may be anchored to the same underlying process such
 523 that one may know about the offset between the two.¹¹ For approaches to this

¹¹For example, in the special case where we have two simultaneously measured data sets with $u = 2$ and 1 time step offset could be combined to give a dataset that has no subsampling.

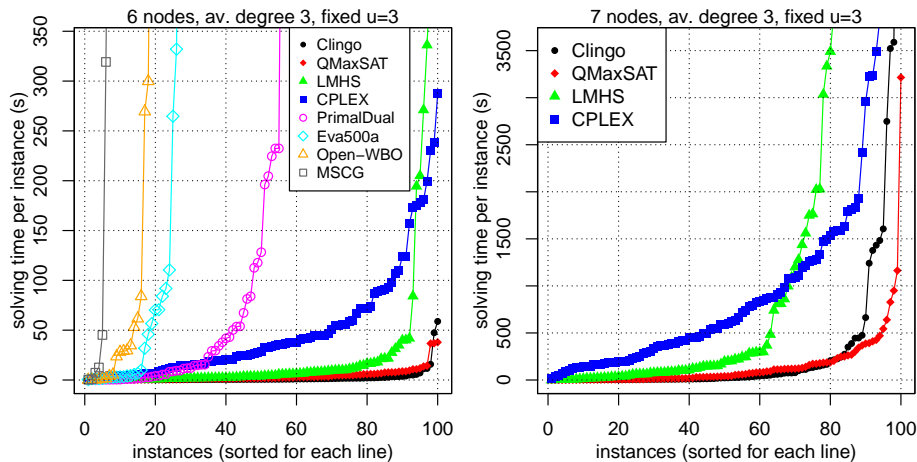


Figure 11: Comparison of running times for different solvers finding the optimal graph.

524 case see Tank et al. [36], who treat this issue as a missing data problem in a
 525 parametric setting. The second case we consider here is one where the subsam-
 526 pled time series are taken at different times and cannot be coordinated to the
 527 same instance of an underlying time series. A natural question is how much
 528 more can be learned by integrating information from multiple sampling rates.
 529 If one sampling rate is an integer multiple of the other, then (provably) noth-
 530 ing additional can be learned. A more interesting situation arises when neither
 531 sampling rate is a multiple of the other. For example, suppose the causal system
 532 operates at a 1-second timescale. If the system is measured every 2 seconds in
 533 one dataset, and every 3 seconds in another dataset, then we have $u_1 = 2/3 \cdot u_2$.
 534 More generally, if u_1/u_2 is non-integer, then when (if ever) is the equivalence
 535 class of \mathcal{G}^1 that satisfies both \mathcal{H}_1 & \mathcal{H}_2 smaller than the equivalence class
 536 for either \mathcal{H} individually? We can start to answer this question using the constraint
 537 satisfaction approach of this paper with only minor modifications.

538 For example, suppose the true system timescale structure is given in Fig-
 539 ure 12a. That is, the system includes four independent time series with self
 540 loops. Undersampling does not change this graph, so the measurement timescale
 541 structures for $u = 2$ and for $u = 3$ will also be the graph in Figure 12a. For this
 542 measurement timescale graph, the system timescale structure is not uniquely
 543 determined for either $u = 2$ or $u = 3$: for example, the system timescale struc-
 544 ture in Figure 12b produces Figure 12a with $u = 2$, and Figure 12c produces
 545 Figure 12a with $u = 3$. In fact, *any* system timescale edge can be present or
 546 absent given either of the measurement timescale graphs alone.¹² However, if
 547 this measurement timescale graph is found at *both* $u = 2$ and $u = 3$, then the
 548 system timescale structure can be uniquely determined: Figure 12b produces

¹²The node labels in Figure 12b and c can be permuted.

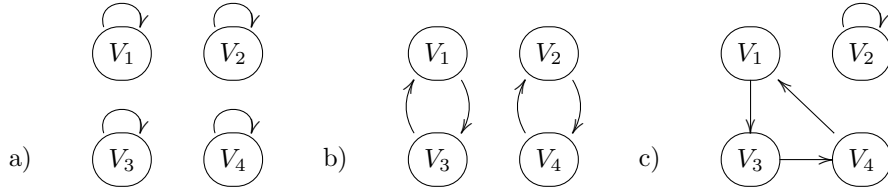


Figure 12: Example graphs. See text for details.

549 a different measurement timescale graph for $u = 3$ and Figure 12c produces
 550 a different measurement timescale graph for $u = 2$. And of course, the same
 551 observations hold if the us are multiplied by a constant (e.g., if $u = 4$ and $u = 6$).

552 To examine the prevalence of this phenomenon, we exhaustively considered
 553 all $65536 (= 2^{4 \cdot 4})$ different 4-variable \mathcal{G}^1 s, and compared the number of equiv-
 554 alence classes given input at a single subsampling rate, versus given inputs at
 555 two subsampling rates. A greater number of equivalence classes means a higher
 556 chance that a random graph will be uniquely identifiable, and so the number of
 557 equivalence classes is an approximate (inverse) measure of the extent of under-
 558 determination.

559 For input at a single undersampling rate, we have $u = 2 \Rightarrow 24265$ equivalence
 560 classes; $u = 3 \Rightarrow 7544$ equivalence classes; and $u = 4 \Rightarrow 3964$ equivalence classes.
 561 These results with a single undersampled input graph thus replicate the known
 562 result that underdetermination is a significant problem, and it rapidly worsens
 563 as u increases [30, 31].

564 If we instead have measurement timescale graphs for both $u = 2, 3$, then
 565 we have 26720 equivalence classes, which is only slightly more than the number
 566 for $u = 2$ by itself. That is, underdetermination is not substantially reduced
 567 if we additionally measure at $u = 3$ when we already have measurements at
 568 $u = 2$. Similarly, for $u = 3, 4$ we have 7814 equivalence classes; again, there is
 569 a reduction in underdetermination compared to $u = 3$ by itself, but it is quite
 570 small. This analysis assumes that all \mathcal{G}^1 are equally likely, and it is an open
 571 question whether measurements at different undersampling rates would have
 572 more impact for certain classes of \mathcal{G}^1 (e.g., connected graphs).

573 9. Discussion

574 We have assumed that all common causes of measured variables are them-
 575 selves measured, but this assumption is frequently violated in real-world data.
 576 Constraint satisfaction methods have elsewhere been used with success to iden-
 577 tify causal relations in the presence of unobserved common causes or latent
 578 variables [16, 23]. For time series data, dropping the assumption of causal suf-
 579 ficiency (in the system timescale) generates complications. Even if the system
 580 timescale process including latent variables is assumed to be first order Markov,
 581 the Markov order of the measurement timescale (naturally without the latent

582 variables) can be arbitrarily larger.¹³ That is, variables arbitrarily far in the
 583 past can (directly in the measurement timescale) cause variables at the current
 584 timestep. We would thus need to both enrich the notation for \mathcal{G}^u to encode the
 585 time lags of direct causal effects, and also modify the statistical tests used to
 586 estimate these connections.

587 Moreover, there can be more information contained in the pattern of time
 588 lags (i.e., *which* past variables directly cause the present) than is given by the
 589 Markov order of the system. As just one example, suppose $\{X^{t-2}, X^{t-4}, \dots\} \rightarrow$
 590 Y^t . The simplest (in terms of number of latents) structure that explains these
 591 influences (i) has a latent L through which X influences Y (i.e., $X^{t-2} \rightarrow L^{t-1} \rightarrow$
 592 Y^t); and (ii) L is part of a 2-loop with another latent M (i.e., $L^{t-1} \rightarrow M^t$ and
 593 $L^t \leftarrow M^{t-1}$). In contrast, if we have $\{X^{t-2}, X^{t-3}, \dots\} \rightarrow Y^t$, then the simplest
 594 structure has only a single latent L through which X influences Y , but where L
 595 has a self-loop (i.e., $L^{t-1} \rightarrow L^t$). The pattern of time lags for direct causes—
 596 in particular, the absence of certain time lags—thus contains information about
 597 the number and causal structure of the latent variables. Estimation of this
 598 pattern, however, can be quite complex statistically.

599 Subsampled time series data is particularly prone to violations of faithful-
 600 ness. For example, the underlying process unrolled over time may include di-
 601 rected paths over many time steps that do not result in significant statistical
 602 dependence in the observed data. In addition, variables observed over subse-
 603 quent time steps might be almost deterministically related. If $V_1^{t-1} \approx V_1^{t-2}$,
 604 then conditioning on V_1^{t-2} may render the statistical dependence through $V_2^t \leftarrow$
 605 $V_1^{t-1} \rightarrow V_3^t$ undetectable from any realistic sample sizes. In the current frame-
 606 work, both of these situations are treated as estimation errors in \mathcal{H} . Further
 607 modeling of these complications may help to achieve improved accuracy.

608 10. Conclusion

609 In this paper, we introduced a constraint optimization based solution for the
 610 problem of learning causal timescale structures from subsampled measurement
 611 timescale graphs and data. Our approach considerably improves the state-of-
 612 art; in the simplest case (subsampling rate $u = 2$), we extended the scalability
 613 by several orders of magnitude. Moreover, our method generalizes to handle
 614 different or unknown subsampling rates in a computationally efficient manner.
 615 Unlike previous methods, our method can operate directly on finite sample in-
 616 put, and we presented approaches that recover, in an optimal way, from conflicts
 617 arising from statistical errors. We demonstrated the accuracy, robustness and
 618 scalability of the approach through a series of simulations and applied it to
 619 real-world time series data. We expect that this considerably simpler approach
 620 will allow for the relaxation of additional model space assumptions in the fu-
 621 ture. In particular, we plan to use this framework to learn the system timescale

¹³This complication is independent of undersampling, and arises even if $u = 1$.

622 causal structure from subsampled data when latent time series confound our
623 observations.

624 Acknowledgments

625 AH was supported by Academy of Finland Centre of Excellence in Com-
626 putational Inference Research COIN (grant 251170) and Academy of Finland
627 grant 295673. SP was supported by NSF IIS-1318759 & NIH R01EB005846. MJ
628 was supported by COIN (grant 251170) and Academy of Finland grants 276412,
629 284591; and Research Funds of the University of Helsinki. FE was supported by
630 NSF 1564330. DD was supported by NSF IIS-1318815 & NIH U54HG008540
631 (from the National Human Genome Research Institute through funds provided
632 by the trans-NIH Big Data to Knowledge (BD2K) initiative). The content is
633 solely the responsibility of the authors and does not necessarily represent the
634 official views of the National Institutes of Health.

635 References

- 636 [1] Ansótegui C, Gabàs J. Solving (weighted) partial MaxSAT with ILP. In:
637 Gomes CP, Sellmann M, editors. Proc. CPAIOR. Springer; volume 7874 of
638 *Lecture Notes in Computer Science*; 2013. p. 403–9.
- 639 [2] Audemard G, Simon L. Predicting learnt clauses quality in modern SAT
640 solvers. In: Boutilier C, editor. Proc. IJCAI. 2009. p. 399–404.
- 641 [3] Biere A. Splatz, Lingeling, Plingeling, Treengeling, YalSAT entering the
642 SAT Competition 2016. In: Balyo T, Heule M, Järvisalo M, editors. Proc. of
643 SAT Competition 2016 – Solver and Benchmark Descriptions. University
644 of Helsinki; volume B-2016-1 of *Department of Computer Science Series of*
645 *Publications B*; 2016. p. 44–5.
- 646 [4] Biere A, Heule M, van Maaren H, Walsh T, editors. Handbook of Satisfia-
647 bility; volume 185 of *FAIA*. IOS Press; 2009.
- 648 [5] Bjørner N, Narodytska N. Maximum satisfiability using cores and correc-
649 tion sets. In: Yang Q, Wooldridge M, editors. Proc. IJCAI. AAAI Press;
650 2015. p. 246–52.
- 651 [6] Danks D, Plis S. Learning causal structure from undersampled time series.
652 In: NIPS 2013 Workshop on Causality. 2013. .
- 653 [7] Dash D, Druzdzel M. Caveats for causal reasoning with equilibrium models.
654 In: Proc. ECSQARU. Springer; volume 2143 of *LNCS*; 2001. p. 192–203.
- 655 [8] Davies J, Bacchus F. Exploiting the power of MIP solvers in MAXSAT.
656 In: Järvisalo M, Gelder AV, editors. Proc. SAT. Springer; volume 7962 of
657 *Lecture Notes in Computer Science*; 2013. p. 166–81.

- 658 [9] Entner D, Hoyer P. On causal discovery from time series data using FCI.
659 Proc PGM 2010;:121–8.
- 660 [10] Gebser M, Kaufmann B, Kaminski R, Ostrowski M, Schaub T, Schneider
661 M. Potassco: The Potsdam answer set solving collection. AI Communica-
662 tions 2011;24(2):107–24.
- 663 [11] Gong M, Zhang K, Schoelkopf B, Tao D, Geiger P. Discovering tempo-
664 ral causal relations from subsampled data. In: Proc. ICML. JMLR.org;
665 volume 37 of *JMLR W&CP*; 2015. p. 1898–906.
- 666 [12] Granger C. Investigating causal relations by econometric models and cross-
667 spectral methods. *Econometrica* 1969;37(3):424–38.
- 668 [13] Granger C. Testing for causality: a personal viewpoint. *Journal of Eco-
669 nomic Dynamics and Control* 1980;2:329–52.
- 670 [14] Granger C. Some recent development in a concept of causality. *Journal of
671 Econometrics* 1988;39(1):199–211.
- 672 [15] Hamilton J. Time series analysis. volume 2. Princeton University Press,
673 1994.
- 674 [16] Hyttinen A, Eberhardt F, Järvisalo M. Constraint-based causal discovery:
675 Conflict resolution with answer set programming. In: Proc. UAI. AUAI
676 Press; 2014. p. 340–9.
- 677 [17] Hyttinen A, Plis S, Järvisalo M, Eberhardt F, Danks D. Causal discovery
678 from subsampled time series data by constraint optimization. In: Antonucci
679 A, Corani G, de Campos CP, editors. Proc. PGM. JMLR.org; volume 52
680 of *JMLR Workshop and Conference Proceedings*; 2016. p. 216–27.
- 681 [18] Hyvärinen A, Zhang K, Shimizu S, Hoyer P. Estimation of a structural
682 vector autoregression model using non-gaussianity. *Journal of Machine
683 Learning Research* 2010;11:1709–31.
- 684 [19] Iwasaki Y, Simon H. Causality and model abstraction. *Artificial Intelli-
685 gence* 1994;67(1):143–94.
- 686 [20] Koshimura M, Zhang T, Fujita H, Hasegawa R. Qmaxsat: A partial max-
687 sat solver. *Journal of Satisfiability, Boolean Modeling and Computation*
688 2012;8(1/2):95–100.
- 689 [21] Kutz M. The complexity of Boolean matrix root computation. *Theoretical
690 Computer Science* 2004;325(3):373–90.
- 691 [22] Lütkepohl H. New introduction to multiple time series analysis. Springer
692 Science & Business Media, 2005.
- 693 [23] Magliacane S, Claassen T, Mooij JM. Ancestral causal inference. In:
694 Proc. NIPS. 2016. .

- 695 [24] Margaritis D, Bromberg F. Efficient Markov network discovery using par-
696 ticle filters. *Computational Intelligence* 2009;25(4):367–94.
- 697 [25] Martins R, Manquinho VM, Lynce I. Open-WBO: A modular MaxSAT
698 solver. In: Sinz C, Egly U, editors. *Proc. SAT*. Springer; volume 8561 of
699 *Lecture Notes in Computer Science*; 2014. p. 438–45.
- 700 [26] Morgado A, Ignatiev A, Marques-Silva J. MSCG: Robust core-guided
701 MaxSAT solving. *Journal on Satisfiability, Boolean Modeling and Com-
702 putation* 2015;9:129–34.
- 703 [27] Narodytska N, Bacchus F. Maximum satisfiability using core-guided
704 maxsat resolution. In: Brodley CE, Stone P, editors. *Proc. AAAI*. AAAI
705 Press; 2014. p. 2717–23.
- 706 [28] Niemelä I. Logic programs with stable model semantics as a constraint
707 programming paradigm. *Annals of Mathematics and Artificial Intelligence*
708 1999;25(3-4):241–73.
- 709 [29] Peters J, Janzing D, Schölkopf B. Causal inference on time series using re-
710 stricted structural equation models. In: Burges CJC, Bottou L, Welling M,
711 Ghahramani Z, Weinberger KQ, editors. *Proc. NIPS 26*. Curran Associates,
712 Inc.; 2013. p. 154–62.
- 713 [30] Plis S, Danks D, Freeman C, Calhoun V. Rate-agnostic (causal) structure
714 learning. In: *Proc. NIPS*. Curran Associates, Inc.; 2015. p. 3285–93.
- 715 [31] Plis S, Danks D, Yang J. Mesochronal structure learning. In: *Proc. UAI*.
716 AUAI Press; 2015. p. 702–11.
- 717 [32] Saikko P, Berg J, Järvisalo M. LMHS: A SAT-IP hybrid MaxSAT solver.
718 In: Creignou N, Berre DL, editors. *Proc. SAT*. Springer; volume 9710 of
719 *Lecture Notes in Computer Science*; 2016. p. 539–46.
- 720 [33] Simons P, Niemelä I, Soinen T. Extending and implementing the stable
721 model semantics. *Artificial Intelligence* 2002;138(1-2):181–234.
- 722 [34] Sonntag D, Järvisalo M, Peña J, Hyttinen A. Learning optimal chain graphs
723 with answer set programming. In: *Proc. UAI*. AUAI Press; 2015. p. 822–31.
- 724 [35] Spirtes P, Glymour C, Scheines R. *Causation, prediction, and search*.
725 Springer, 1993.
- 726 [36] Tank A, Fox E, Shojaie A. Identifiability of non-Gaussian structural VAR
727 models for subsampled and mixed frequency time series. In: *SIGKDD*
728 *Workshop on Causal Discovery*. 2016. .
- 729 [37] Wei W. *Time series analysis*. Addison-Wesley, 1994.